

# The geography of semidiurnal mode-1 internal-tide energy loss

S. M. Kelly,<sup>1,2</sup> N. L. Jones,<sup>1</sup> J. D. Nash,<sup>3</sup> and A. F. Waterhouse<sup>4</sup>

Received 10 July 2013; accepted 13 August 2013; published 5 September 2013.

[1] The semidiurnal mode-1 internal tide receives 0.1–0.3 TW from the surface tide and is capable of propagating across ocean basins. The ultimate fate of mode-1 energy after long-distance propagation is poorly constrained by existing observations and numerical simulations. Here, global results from a two-dimensional semi-analytical model indicate that topographic scattering is inefficient at most locations deeper than 2500 m. Next, results from a one-dimensional linear model with realistic topography and stratification create a map of mode-1 scattering coefficients along the continental margins. On average, mode-1 internal tides lose about 60% of their energy upon impacting the continental margins: 20% transmits onto the continental shelf, 40% scatters to higher modes, and 40% reflects back to the ocean interior. These analyses indicate that the majority of mode-1 energy is likely lost at large topographic features (e.g., continental slopes, seamounts, and mid-ocean ridges), where it may drive elevated turbulent mixing. **Citation:** Kelly, S. M., N. L. Jones, J. D. Nash, and A. F. Waterhouse (2013), The geography of semidiurnal mode-1 internal-tide energy loss, *Geophys. Res. Lett.*, 40, 4689–4693, doi:10.1002/grl.50872.

## 1. Introduction

[2] Large-scale tides in the deep ocean propagate as linear shallow-water waves that are classified by vertical mode number ( $n \geq 0$ ) [Wunsch, 1975]. The mode-0 tide (i.e., the surface tide) propagates at  $\mathcal{O}(100 \text{ m s}^{-1})$ , whereas higher-mode tides (i.e., the internal tides) propagate with group speeds of  $\mathcal{O}(\leq 1 \text{ m s}^{-1})$ . Semidiurnal-tide energy originates in mode 0, via 2.4 TW of work by the astronomical tide-generating force, and either dissipates through friction in shallow seas (1.6 TW) [Egbert and Ray, 2000] or cascades to higher modes through topographic internal-tide generation [Garrett and Kunze, 2007]. In regions of internal-tide generation, low modes are observed to radiate [Ray and Mitchum, 1996] and high modes are observed to locally dissipate [Klymak et al., 2008]. At the Mid-Atlantic and Hawaiian Ridges, 12% [Zilberman et al., 2009] and 35% [Zhao et al., 2011] of the total surface-tide energy loss, respectively, are transferred to the mode-1 internal tide (the variability being due to “rough” versus “abrupt” topography). Extrapolating

these results to the global ocean suggests that the semidiurnal mode-1 internal tide receives 0.1–0.3 TW of energy from the surface tide. The ultimate fate of this energy, which is presently unknown, is relevant to the general circulation of the ocean [Munk and Wunsch, 1998; Melet et al., 2013], biological production along the continental margins [Sharples et al., 2009], and the design of offshore structures [Osborne et al., 1978].

[3] Observational analyses by Wunsch [1975] and Alford and Zhao [2007a] indicate that the average open-ocean semidiurnal internal-tide energy density is about  $1000 \text{ J m}^{-2}$ . If 50% of the internal-tide energy is in mode 1 (an upper bound based on modal decompositions near abrupt topography) [e.g., Nash et al., 2006], then mode-1 energy density is  $500 \text{ J m}^{-2}$ . Combining energy density and power produces a semidiurnal mode-1 decay timescale of

$$\tau = \frac{500 \text{ J m}^{-2} \times (\text{area of the oceans})}{0.1\text{--}0.3 \text{ TW}} = 7\text{--}21 \text{ days} . \quad (1)$$

For  $\tau = \mathcal{O}(10 \text{ days})$ , the mode-1 internal tides are unaffected by nonlinear interactions [St. Laurent and Garrett, 2002], because they have large group speeds (e.g.,  $2\text{--}3 \text{ m s}^{-1}$ ) [Alford and Zhao, 2007b] and small Froude numbers (even when impinging on tall and steep ridges) [Klymak et al., 2013].

[4] Assuming a group speed of  $2.5 \text{ m s}^{-1}$ , mode-1 internal tides have a range of 1500–4500 km, allowing them to interact with both small- and large-scale topography. Regional studies have indicated that linear topographic scattering dominates energy loss from the mode-1 internal tide [Johnston et al., 2003; Klymak et al., 2011; Kelly et al., 2012]. Here we calculate topographic scattering coefficients at (i) depths greater than 2500 m in the interior of the ocean basins (section 2) and (ii) continental-slope topography at the perimeter of the ocean basins (section 3) to assess where the majority of mode-1 energy dissipation likely occurs (section 4).

## 2. Scattering by Small-Scale Topography

[5] As mode-1 internal tides propagate across ocean basins, they interact with small-scale topographic bumps, which scatter energy to higher-mode internal tides [e.g., Bühler and Holmes-Cerfon, 2011]. Nycander [2005] derived a semi-analytical model to estimate surface-tide scattering using surface-tide velocities. Here we use near-bottom mode-1 velocities in this model to estimate mode-1 scattering. Because the global distribution of near-bottom mode-1 velocity is unknown, mode-1 scattering at each grid cell is divided by an incident mode-1 energy flux to produce a scattering coefficient

$$S_{\text{interior}} = \frac{(P_+ + P_-) \times \text{area}}{F \times 1/2 \text{ perimeter}} , \quad (2)$$

<sup>1</sup>The Oceans Institute and School of Environmental Systems Engineering, University of Western Australia, Crawley, Western Australia, Australia.

<sup>2</sup>Now at Department of Mechanical Engineering, Massachusetts Institute of Technology, Cambridge, Massachusetts, USA.

<sup>3</sup>College of Oceanic and Atmospheric Sciences, Oregon State University, Covallis, Oregon, USA.

<sup>4</sup>Scripps Institution of Oceanography, La Jolla, California, USA.

Corresponding author: S. M. Kelly, Department of Mechanical Engineering, Massachusetts Institute of Technology, 7-321, 77 Massachusetts Ave., Cambridge, MA 02139, USA. (samkelly@mit.edu)

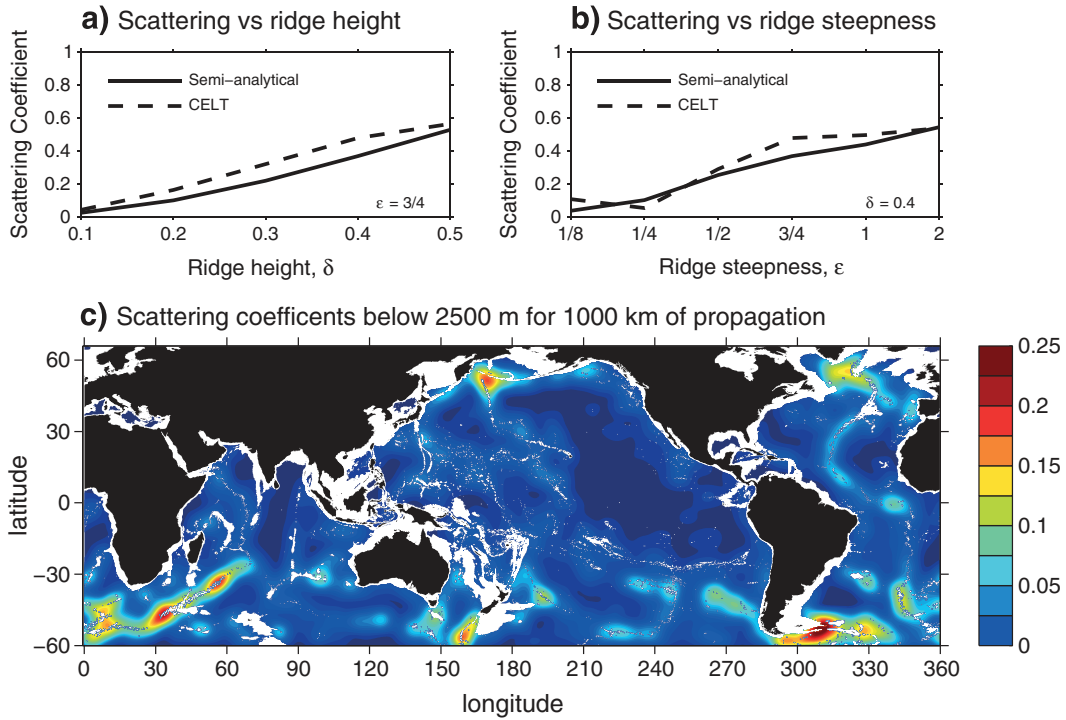


**Figure 1.** Semi-analytical (solid) and CELT (dashed) scattering coefficients for a Witch of Agnesi ridge with topographic resolution  $\Delta x = b/10$  and (a) variable height,  $\delta$ , and (b) steepness,  $\epsilon$  (see *Garrett and Kunze* [2007] for the exact definitions of the topographic parameters). (c) Mode-1 scattering coefficients,  $S_{\text{interior}}$ , per 1000 km of propagation at depths greater than 2500 m.

where  $P_+$  and  $P_-$  [ $\text{W m}^{-2}$ ] are the scattering expressions derived by *Nycander* [2005], the area and perimeter refer to that of each computational grid cell, and  $F = (1+r)\rho_0 H c_1 (1/2)(U_+^2 + U_-^2)/\phi_1^2|_{z=-H}$  [ $\text{W m}^{-1}$ ] is the depth-integrated energy flux produced by a freely-propagating mode-1 internal tide with semi-major (semi-minor) near-bottom velocities  $U_+$  ( $U_-$ ). In the definition of  $F$ ,  $r$  is the ratio of potential to kinetic energy [ $(\omega^2 - f^2)/(\omega^2 + f^2)$ , where  $\omega$  and  $f$  are the tidal and inertial frequency, respectively],  $\rho_0$  is reference density,  $H$  is depth, and  $c_1$  and  $\phi_1|_{z=-H}$  are the local mode-1 group speed and structure function evaluated at the bottom [see, e.g., *Kelly et al.*, 2013]. Because this model is based on linear dynamics, (2) is independent of the strength of the internal tide (i.e.,  $U_+$  and  $U_-$ ).

[6] *Nycander's*, 2005 model assumes that the topography has short wavelength (with respect to the forcing), is subcritical (i.e., nonsteep), and small amplitude (although it does include a heuristic filter to account for finite depth). To identify the practical limitations of the semi-analytical model, we compare mode-1 scattering coefficients obtained via (2) with those calculated via the Coupling Equations for Linear Tides model (CELT; see the next section) [*Kelly et al.*, 2013], which does not require assumptions about topographic height or steepness. Semi-analytical scattering coefficients integrated over a suite of Witch of Agnesi ridges (i.e., all combinations of  $\delta = 0.1, 0.2, 0.3, 0.4, 0.5$  and  $\epsilon = 1/8, 1/4, 1/2, 3/4, 1, 2$ ) [see *Garrett and Kunze*, 2007] show a broad agreement with CELT coefficients (Figures 1a and 1b). For subcritical ridges that are shorter than half the water depth, semi-analytical scattering coefficients are only slightly different than CELT coefficients (i.e., they are smaller by  $0.04 \pm 0.06$ ); therefore, (2) is well suited

for mapping scattering coefficients below 2500 m, where large-amplitude topography is eliminated a priori and only 6% of topographic slopes (calculated at 2-min resolution) are supercritical.

[7] A global map of  $S_{\text{interior}}$  is computed following the exact numerical methods of *Nycander* [2005] (Figure 1c). Near-bottom stratification  $N^2(z)$  and 2-min bathymetry  $H(x, y)$  are obtained from the World Ocean Atlas and General Bathymetric Chart of the Oceans.  $S_{\text{interior}}$  is calculated at 2 min resolution and then smoothed and summed over 1000 km. The result quantifies the fraction of incident mode-1 energy flux that is lost to scattering along a 1000-km ray path, with arbitrary orientation, that is centered at each grid point. Scattering coefficients can be applied iteratively for longer ray paths, i.e., scattering coefficients over 4000-km ray paths are roughly  $4\times$  the scattering coefficients reported here.

[8] Results indicate that scattering coefficients are generally  $<10\%$ , but can be significant along mid-ocean ridges (although ridge peaks shallower than 2500 m are excluded), where the model predicts up to 25% of energy flux is scattered per 1000 km of propagation (Figure 1c). Small coefficients in the eastern Pacific are consistent with in situ observations, which indicate that mode-1 internal tides do not lose measurable energy as they propagate north from Hawaii [*Alford et al.*, 2007].

### 3. Scattering by Large-Scale Topography

[9] To examine mode-1 internal-tide scattering along the continental margins, we employ CELT, which is a linear, energy conserving, and numerically inexpensive tool

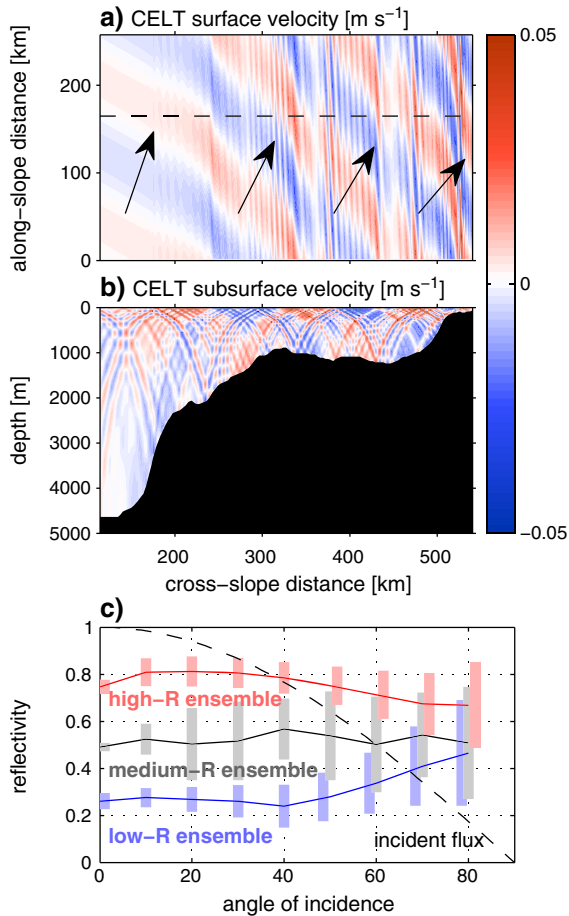


**Figure 2.** CELT (a) surface and (b) subsurface velocities show the refraction of a mode-1 internal tide incident on the Australian North West Slope at  $60^\circ$ . Arrows (a) illustrate the angle of propagation at various locations. The dashed line in (a) indicates the location of the cross-shelf profile in (b). (c) Ensemble-averaged  $R$ 's (lines) and ensemble standard deviations (bars) depend on angle of incidence. Ensembles consist of 10 slopes with normal reflectivities of  $R = 0.25 \pm 0.05$  (blue),  $0.5 \pm 0.05$  (gray), and  $0.75 \pm 0.05$  (red). The dashed line (c) indicates the fraction of incident mode-1 energy flux in the cross-slope direction.

for assessing internal-tide scattering [Kelly *et al.*, 2013]. CELT incorporates realistic stratification, topography, and planetary rotation, but is limited to one horizontal dimension. Therefore, the model is only employed on continental slopes, which are often approximately along-slope uniform. The continental margins are divided into 989 cross sections of continental slope, which are input into CELT to determine the fraction of incident mode-1 energy flux that is reflected to the deep ocean in mode-1 ( $R$ ), transmitted onto the shelf in mode-1 ( $T$ ), and scattered to modes  $n > 1$  ( $S$ ).

[10] Topographic cross sections of the continental slope are identified by low-pass filtering  $H(x, y)$  with a 100 km cutoff wavelength and calculating the normal angle every 100 km along the 1000-m isobath. Once the orientation is determined, the cross sections are defined with full-resolution  $H$ . CELT is configured with a unit amplitude normally incident mode-1 internal tide, horizontally-variable

$N^2(z)$ , 16 vertical modes, 2-km horizontal resolution, zero viscosity, and radiation boundary conditions. The continental shelves are truncated at the 175-m isobath.

### 3.1. Obliquely Incident Scattering

[11] Some locations along the continental margins receive an incident mode-1 internal tide at an oblique angle, which alters local reflection and scattering dynamics [e.g., Martini *et al.*, 2011; Kelly *et al.*, 2012]. Here we extend CELT to include an obliquely incident mode-1 internal tide by conserving the incident along-slope wavenumber [Chapman and Hendershott, 1981]. The condition causes obliquely incident tides to refract toward shallower water, like surface waves on a beach (Figures 2a and 2b).

[12] The sensitivity of  $R$  to the angle of incidence is examined for three ensembles of 10 realistic continental slopes. The ensembles are chosen to have normal reflectivities of  $R = 0.25 \pm 0.05$ ,  $0.5 \pm 0.05$ , and  $0.75 \pm 0.05$  (Figure 2c). For angles of incidence  $< 60^\circ$ , the ensemble-averaged  $R$ 's do not have strong biases and ensemble standard deviations are less than  $\pm 0.15$ . Reflection at more oblique angles is less important to the global energy balance because a smaller fraction of total internal-tide energy flux is actually incident on (i.e., normal to) the slope. These results indicate that a global map of  $R$  based on normally-incident mode-1 internal tides is largely applicable, even over slopes that receive obliquely incident internal tides.

### 3.2. Scattering at the Continental Margins

[13] Results from CELT simulations around the globe indicate that  $R$ ,  $T$ , and  $S$  vary on local and regional scales (Figure 3). The variation in coefficients between adjacent cross sections is an indication of unresolved one- and two-dimensional topography and suggests that individual coefficients have uncertainties of approximately  $\pm 0.2$ . However,  $R$ ,  $T$ , and  $S$  are also sensitive to the regional shapes of the continental slopes. For instance,  $R$  is highest where the continental slopes are steep (i.e., supercritical), at locations such as Madagascar, southern Australia, Brazil, and northeastern North America (Figure 3a). Conversely,  $T$  is highest where continental slopes are less steep (i.e., subcritical), at locations such as southwest Africa, northwest Australia, and Argentina (Figure 3b).  $S$  is substantial almost everywhere and is particularly enhanced along the west coasts of North and South America, which have continental slopes that are near critical (Figure 3c). Despite overarching trends,  $R$ ,  $T$ , and  $S$  depend on the spatial distribution of slope steepness, height, and curvature and are not easily explained via trivial functions of slope steepness.

[14] Basin averaged  $R$ ,  $T$ , and  $S$  vary by 20% between oceans (Table 1). In contrast to  $S_{\text{interior}}$ , the western Pacific continental slopes have lower scattering efficiencies (and higher reflectivities) than the those in the eastern Pacific, suggesting that the eastern and western Pacific may have slightly different mode-1 energy pathways. Global averages indicate that only 40% of incident mode-1 energy flux is reflected from the continental margins in mode 1 (Table 1). The remaining mode-1 energy flux is scattered to higher modes (40%) or transmitted past the 175 m isobath (20%). Approximately one fourth of the incident energy is scattered into modes  $n \geq 4$  ( $S_{n \geq 4}$ ), which, because of their slow propagation and high vertical shear, are likely to dissipate locally [St. Laurent and Garrett, 2002; Klymak *et al.*, 2013].

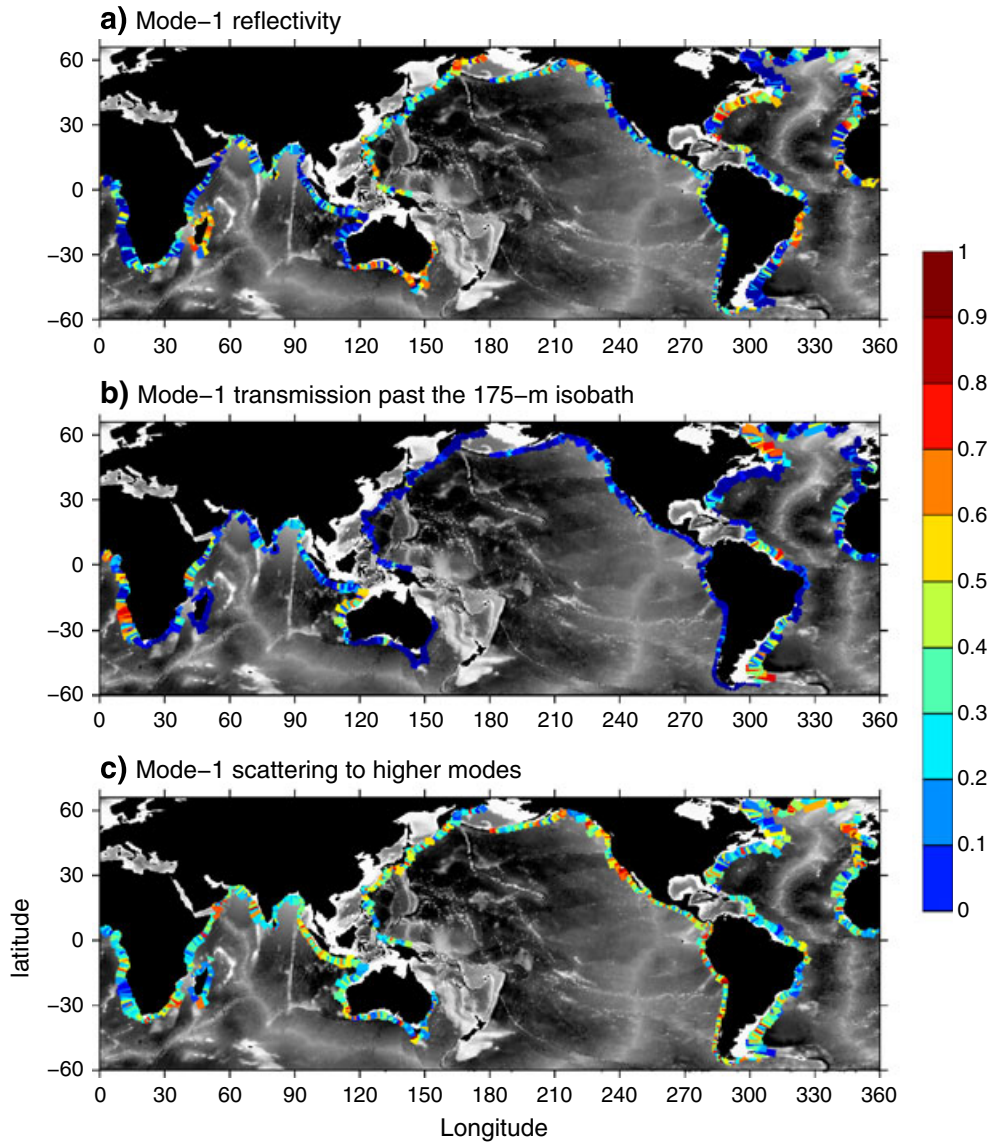


**Figure 3.** Global distribution of the fraction of an incident mode-1 internal-tide energy flux that is (a) reflected ( $R$ ) in mode-1, (b) transmitted ( $T$ ) past the 175 m isobath in mode-1, and (c) scattered ( $S$ ) to higher modes.

**4. Discussion**

[15] Bulk observations indicate that mode-1 internal tides can propagate 1500–4500 km through the deep ocean. Analyses here suggest that (i) topographic scattering at depths >2500 m is unlikely to explain the majority of mode-1 energy loss and (ii) about two thirds of the mode-1 energy flux incident on the continental margins (even at oblique angles) is lost through scattering to higher modes or transmission onto the continental shelf. Due to model limitations, we do not estimate scattering coefficients at seamounts and mid-ocean ridges, which are both tall and two-dimensional; regional studies suggest that scattering at these features is also significant (e.g.,  $S = 0.4$ ) [Johnston *et al.*, 2003]. Therefore, we conclude that mode-1 internal tides probably lose most of their energy by scattering at large, remote, topographic features. This conclusion supports Alford and Zhao’s [2007b] assertion that standing internal tides are not observed in the open ocean because, on average, little energy is reflected at the continental margins. However, results here,

which indicate  $R > 0.5$  on a few continental slopes, also suggest that partially standing internal waves may exist in some regions of the open ocean.

[16] Using a numerical model, Melet *et al.* [2013] showed that ocean circulation is sensitive to the geography and vertical distribution of diapycnal mixing that occurs where internal tides are generated. This mixing is associated with approximately one third of deep-ocean tidal dissipation.

**Table 1.** Regional Averages of Reflection ( $R$ ), Transmission ( $T$ ), Total Scattering ( $S$ ), and Scattering to Modes  $n \geq 4$  ( $S_{n \geq 4}$ ) Coefficients Along the Continental Margins

Ocean	$R$	$T$	$S$	$S_{n \geq 4}$
Atlantic	0.4	0.2	0.4	0.2
Indian	0.3	0.2	0.5	0.2
E. Pacific	0.3	0.1	0.6	0.3
W. Pacific	0.5	0.1	0.4	0.2
Southern	0.5	0.1	0.4	0.2
Global	0.4	0.2	0.4	0.2

The remaining tidal dissipation, which is associated with the demise of radiating internal tides, may have equally important effects on ocean circulation. The maps presented here identify geographic regions where radiating mode-1 internal tides are most likely to scatter to higher modes, dissipate, and drive turbulent mixing. These maps provide global context for (i) detailed regional studies that quantify the spatial patterns of incident internal-tide energy dissipation along continental slopes [e.g., Kelly *et al.*, 2012] and in canyons [e.g., Kunze *et al.*, 2012], and (ii) models that link mode-1 scattering directly to turbulence [e.g., Klymak *et al.*, 2013; S. Legg, manuscript in preparation, 2013]. Global, regional, and fine-scale studies will all be necessary in creating a precise map of where the 0.1–0.3 TW of propagating semidiurnal mode-1 energy is dissipated.

[17] **Acknowledgments.** S.M. Kelly was supported by a postdoctoral fellowship funded through an AIMS-CSIRO-UWA collaborative agreement. J.D. Nash was supported by NSF grant OCE0350543. A.F. Waterhouse was supported by NSF grant OCE-0968721. We thank two anonymous reviewers for their constructive criticism, which improved the manuscript.

[18] The Editor thanks two anonymous reviewers for their assistance in evaluating this paper.

## References

- Alford, M. H., and Z. Zhao (2007a), Global patterns of low-mode internal-wave propagation. Part I: Energy and energy flux, *J. Phys. Oceanogr.*, *37*, 1829–1848, doi:10.1175/JPO3085.1.
- Alford, M. H., and Z. Zhao (2007b), Global patterns of low-mode internal-wave propagation. Part II: Group velocity, *J. Phys. Oceanogr.*, *37*, 1849–1858, doi:10.1175/JPO3086.1.
- Alford, M. H., J. A. MacKinnon, Z. Zhao, R. Pinkel, J. Klymak, and T. Peacock (2007), Internal waves across the Pacific, *Geophys. Res. Lett.*, *34*, L24601, doi:10.1029/2007GL031566.
- Bühler, O., and M. Holmes-Cerfon (2011), Decay of an internal tide due to random topography in the ocean, *J. Fluid Mech.*, *678*, 271–293, doi:10.1017/jfm.2011.115.
- Chapman, D. C., and M. C. Hendershott (1981), Scattering of internal waves obliquely incident upon a step change in bottom relief, *Deep Sea Res., Part A*, *11*, 1323–1338, doi:10.1016/0198-0149(81)90037-6.
- Egbert, G. D., and R. D. Ray (2000), Significant dissipation of tidal energy in the deep ocean inferred from satellite altimeter data, *Nature*, *405*, 775–778, doi:10.1038/35015531.
- Garrett, C., and E. Kunze (2007), Internal tide generation in the deep ocean, *Annu. Rev. Fluid Mech.*, *39*, 57–87, doi:10.1146/annurev.fluid.39.050905.110227.
- Johnston, T. M. S., M. A. Merrifield, and P. E. Holloway (2003), Internal tide scattering at the Line Islands Ridge, *J. Geophys. Res.*, *108*(C11), 3365, doi:10.1029/2003JC001844.
- Kelly, S. M., J. D. Nash, K. I. Martini, M. H. Alford, and E. Kunze (2012), The cascade of tidal energy from low to high modes on a continental slope, *J. Phys. Oceanogr.*, *42*, 1217–1232, doi:10.1175/JPO-D-11-0231.1.
- Kelly, S. M., N. L. Jones, and J. D. Nash (2013), A coupled model for Laplace's tidal equations in a fluid with one horizontal dimension and variable depth, *J. Phys. Oceanogr.*, *43*, 1780–1797, doi:10.1175/JPO-D-12-0147.1.
- Klymak, J. M., R. Pinkel, and L. Rainville (2008), Direct breaking of the internal tide near topography: Kaena Ridge, Hawaii, *J. Phys. Oceanogr.*, *38*, 380–399, doi:10.1175/2007JPO3728.1.
- Klymak, J. M., M. H. Alford, R.-C. Lien, Y. J. Yang, and T.-Y. Tang (2011), The breaking and scattering of the internal tide on a continental slope, *J. Phys. Oceanogr.*, *41*, 926–945, doi:10.1175/2010JPO4500.1.
- Klymak, J. M., M. Buijsman, S. Legg, and R. Pinkel (2013), Parameterizing baroclinic internal tide scattering and breaking on supercritical topography: The one- and two-ridge cases, *J. Phys. Oceanogr.*, *43*, 1380–1397, doi:10.1175/JPO-D-12-061.1.
- Kunze, E., C. MacKay, E. E. McPhee-Shaw, K. Morrice, J. B. Girton, and S. R. Terker (2012), Turbulent mixing and exchange with interior waters on sloping boundaries, *J. Phys. Oceanogr.*, *42*, 910–927, doi:10.1175/JPO-D-11-075.1.
- Martini, K. I., M. H. Alford, E. K. S. M. Kelly, and J. D. Nash (2011), Observations of internal tides on the Oregon Continental Slope, *J. Phys. Oceanogr.*, *41*, 1772–1794, doi:10.1175/2011JPO4581.1.
- Melet, A., R. Hallberg, S. Legg, and K. Polzin (2013), Sensitivity of the ocean state to the vertical distribution of internal-tide driven mixing, *J. Phys. Oceanogr.*, *43*, 602–615, doi:10.1175/JPO-D-12-055.1.
- Munk, W., and C. Wunsch (1998), Abyssal recipes II: Energetics of tidal and wind mixing, *Deep Sea Res.*, *45*, 1977–2010, doi:10.1016/S0967-0637(98)00070-3.
- Nash, J. D., E. Kunze, C. M. Lee, and T. B. Sanford (2006), Structure of the baroclinic tide generated at Kaena Ridge, Hawaii, *J. Phys. Oceanogr.*, *36*, 1123–1135, doi:10.1175/JPO2883.1.
- Nycander, J. (2005), Generation of internal waves in the deep ocean by tides, *J. Geophys. Res.*, *110*, C10028, doi:10.1029/2004JC002487.
- Osborne, A. L., T. L. Burch, and R. I. Scarlet (1978), The influence of internal waves on deep-water drilling, *J. Pet. Tech.*, *30*, 1497–1504, doi:10.2118/6913-PA.
- Ray, R. D., and G. T. Mitchum (1996), Surface manifestation of internal tides generated near Hawaii, *Geophys. Res. Lett.*, *23*, 2101–2104, doi:10.1029/96GL02050.
- Sharples, J., C. M. Moore, A. E. Hickman, P. M. Holligan, J. F. Tweddle, M. R. Palmer, and J. H. Simpson (2009), Internal tide mixing as a control on continental margin ecosystems, *Geophys. Res. Lett.*, *36*, L23603, doi:10.1029/2009GL040683.
- St. Laurent, L., and C. Garrett (2002), The role of internal tides in mixing the deep ocean, *J. Phys. Oceanogr.*, *32*, 2882–2899, doi:10.1175/1520-0485(2002)032<2882:TROITI>2.0.CO;2.
- Wunsch, C. (1975), Internal tides in the ocean, *Rev. Geophys. Space Phys.*, *13*, 167–182, doi:10.1029/RG013i001p00167.
- Zhao, Z., M. H. Alford, J. Girton, T. M. S. Johnston, and G. Carter (2011), Internal tides around the Hawaiian Ridge estimated from multisatellite altimetry, *J. Geophys. Res.*, *116*, C12039, doi:10.1029/2011JC007045.
- Zilberman, N. V., J. M. Becker, M. A. Merrifield, and G. S. Carter (2009), Model estimates of  $M_2$  internal tide generation over Mid-Atlantic Ridge topography, *J. Phys. Oceanogr.*, *39*, 2635–2651, doi:10.1175/2008JPO4136.1.